Supporting Information to the manuscript:

Diffusion of Nanoparticles with Activated Hopping

in Crowded Polymer Solutions

Chundong Xue,[1,4,6] Xinghua Shi,[3,6] Yu Tian,[5] Xu Zheng,[1*] and Guoqing Hu[2*]

[1]State Key Laboratory of Nonlinear Mechanics, Chinese Academy of Sciences, Beijing 100190, China

[2]Department of Engineering Mechanics & State Key Laboratory of Fluid Power and Mechatronic Systems, Zhejiang University, Hangzhou 310027, China

[3]National Center for Nanoscience and Technology of China, Beijing 100190, China

[4]School of Optoelectronic Engineering and Instrumentation Science, Dalian University of Technology, Dalian 116024, China

[5]State Key Laboratory of Tribology, Tsinghua University, Beijing 100084, China

[6]University of Chinese Academy of Sciences, Beijing 100149, China

[*]Corresponding addresses: ghu@zju.edu.cn; zhengxu@lnm.imech.ac.cn
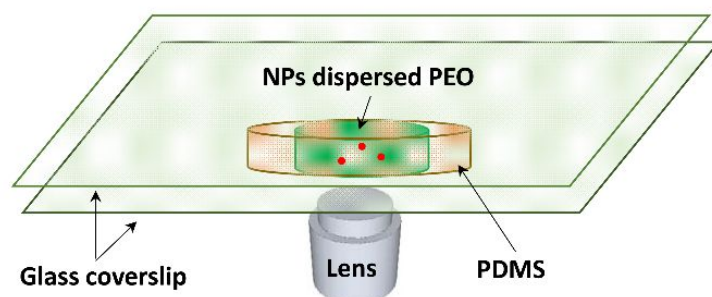
S1 Materials and methods

Figure S1. Schematic of the home-made experimental cell. The cell size is 1 cm in diameter and 2 mm in height. The coverslips and PDMS are bonded using oxygen plasma.
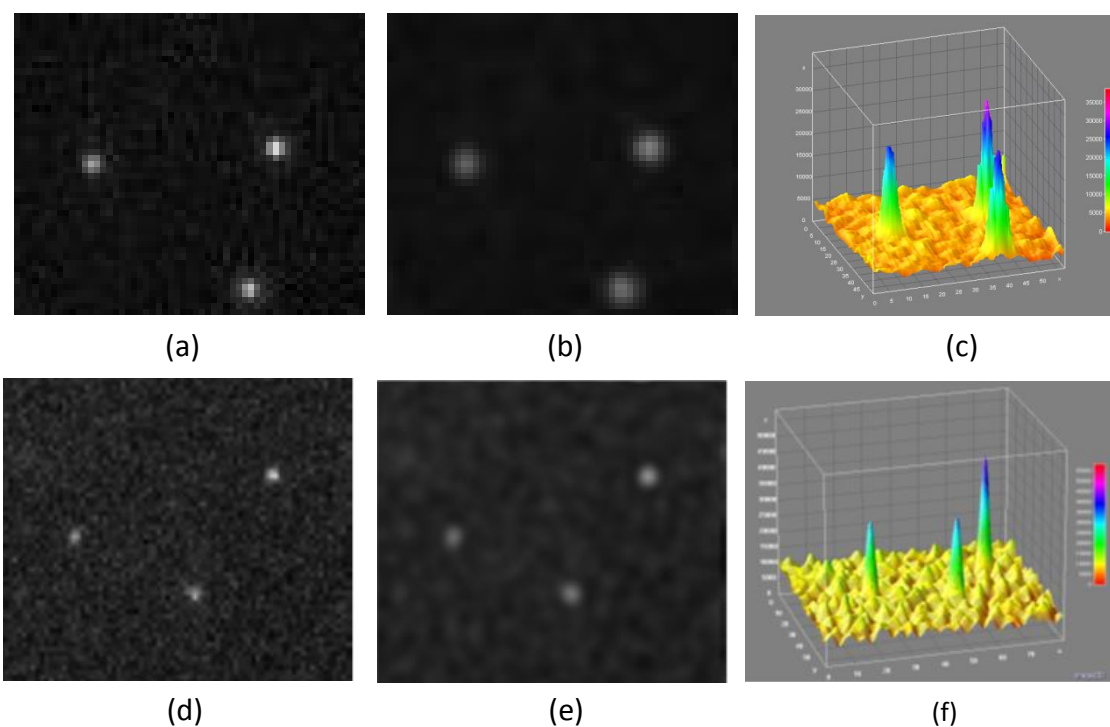

(a) (b) (c)

(d) (e) (f)

Figure S2. The image process of image filtering and particle identification. (a) raw image of three 100 nm NPs; (b) after noise filtering and Gaussian blur, the background noise is lowered and the grey-scale value distribution near each particle region is re-constructed; (c) very sharp peaks of particle grey-scale value distribution, which makes particle identification very easy. (d, e, f) the image process for 40 nm, corresponding to (a, b, c), respectively.

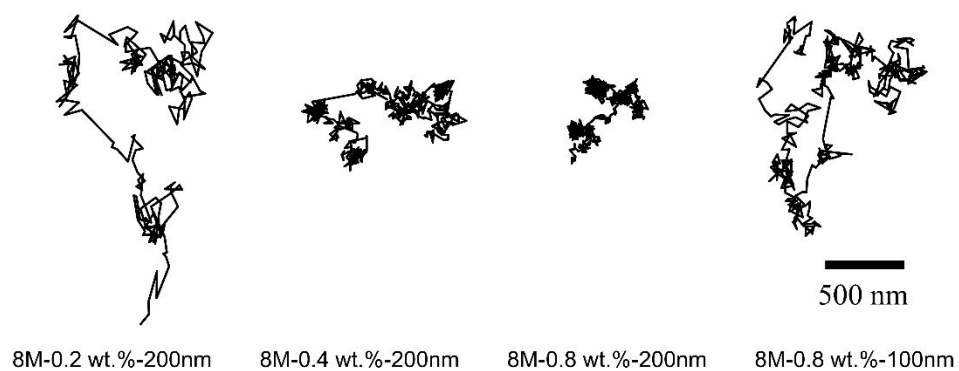8M-0.2 wt.%-200nm   8M-0.4 wt.%-200nm   8M-0.8 wt.%-200nm   8M-0.8 wt.%-100nm

Figure S3. Some typical trajectories of the intermittent long-distance hops. The corresponding Mw, c and NP diameter d are labelled below the trajectories.
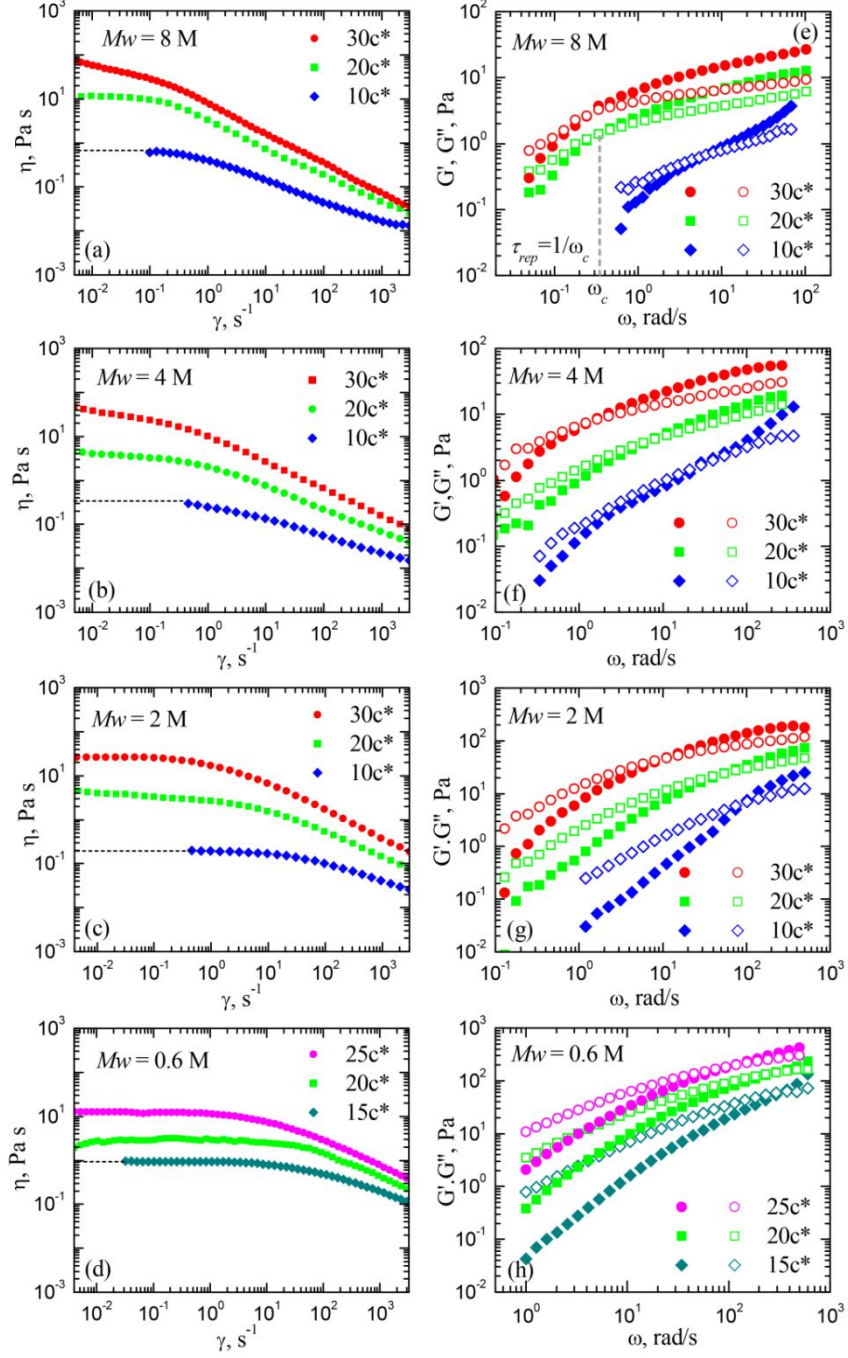
Figure S4. (a) - (d) The measured viscosity η as a function of shear rate γ at three concentrations for 8 M, 4 M, 2 M and 0.6 M PEO solution, respectively. (e)-(f) The measured storage G' and loss G'' moduli corresponding to (a) – (d). The concentration $c*$ is the overlap concentration that are listed in Table S1 below. The zero shear viscosity η_{zs} can be extrapolated from the measured viscosity curve at about $\gamma = 10^{-2}$ s^{-1} for each case. The measured reptation time τ_{rep} was identified $\tau_{rep} = 1/\omega_c$, where ω_c is the angular frequency at $G'/G'' = 1$, as shown in panel (e).

Tube diameter d_t and average mesh size ξ. For PEO solutions, the gyration radius can be obtained using $R_g = 0.02Mw^{0.58}$ [nm],[1] and the overlap concentration is then calculated by $c^* = 3Mw/4\pi R_g^3 N_A$, where N_A is the Avogadro constant.[2] The tube diameter is calculated as $d_t(c) = d_t(1)c^{-v/(3v-1)}$, where $d_t(1) \approx 4$ nm and $v \approx 0.588$ is the Flory exponent. The calculated values of d_t for various Mw and c are listed in Table S1 (note that the concept of tube diameter is only valid for entangle solutions where $c > 7c^*$). To compare, the correlation lengths $\xi = R_g(c/c^*)^{-0.76}$ when $c = 5c^*$ that represent the average mesh size of PEO networks are also listed.[2] From Table S1, we can see that the NP's sizes d in current experiments are usually comparable to or larger than PEO tube diameters d_t, and d are much larger than the average mesh sizes ξ.

Table S1. The calculated values of tube diameters d_t and averages mesh sizes ξ for various Mw and c.

Mw [g/mol]	c^* [wt.%]	d_t [nm]				ξ [nm]
		$10c^*$	$20c^*$	$30c^*$	$40c^*$	$5c^*$
8 M	0.04	251	150	110	89	59
4 M	0.065	175	104	77	62	40
2 M	0.10	126	75	55	45	26
1 M	0.18	81	48	36	29	18
0.6 M	0.26	62	37	27	22	13
0.3 M	0.44	42	25	18	15	9

S2 Determination of reptation time τ_{rep} and plateau modulus G_e

From the measured curves of Figure S4 (viscosity *vs.* shear rate), the "zero shear" viscosity η_{zs} can be approximately extrapolated at very low shear rate (10^{-2} s^{-1}). For each Mw, the values of η_{zs} show similar concentration scaling as $\eta_{zs} \sim c^\beta$, and the exponents of β are consistent with

theoretically predicted value of 3.9.[3] From the measured curves of moduli, we can see that at low frequencies $G'' > G'$ and $G'' \sim \omega$, while at high frequencies $G' > G''$. According to the Maxwell model of a viscoelastic fluid, the measured reptation time τ_{rep} was identified as the reciprocal of the angular frequency ω where $G'/G'' = 1$, as shown in Figure S4e. Some specific values of the measured reptation time τ_{rep} are listed in Table S2, in which the corresponding values of crossover time τ_c are also given for contrast. The measured τ_{rep} for various Mw and c are presented in Figure 2d, where they always show good agreement with the theoretical prediction $\tau_{rep} = \tau_0 N^3/N_e(1)c^{3(1-v)/(3v-1)}$.[3, 4] In this theoretical formula, $\tau_0 \approx 0.2$ ns is the monomer relaxation time at room temperature, $N = (\varepsilon Mw)/M_0$ is the number of Kuhn monomers per chain, and $N_e(1) \approx 14$ is the Kuhn monomer per entanglement in the melt. For PEO, the Kuhn monomer molar mass $M_0 = 140$, and a coefficient $\varepsilon = 0.8$ of the ratio between the actual Mw and the nominal Mw is introduced in actual calculation.

Table S2. Typical values of τ_c and τ_{rep} for 200 nm NP.

Mw [g/mol]		τ [s]		
		$10c^*$	$20c^*$	$30c^*$
8 M	τ_c	0.030	0.16	0.22
	τ_{rep}	0.19	3.03	4.09
2 M	τ_c	0.0043	0.0054	0.023
	τ_{rep}	0.015	0.026	0.11
1 M	τ_c	0.0037	0.0047	0.028
	τ_{rep}	0.0098	0.019	0.052

The plateau modulus G_e was then evaluated as $G_e = \eta_{zs}/\tau_{rep}$.[5-8] The experimentally obtained G_e values are well consistent with the theoretical prediction $G_e = k_B T/L^3$ ($L^3 = d_t\xi^2$),[3, 7, 9] as shown in Figure S5.
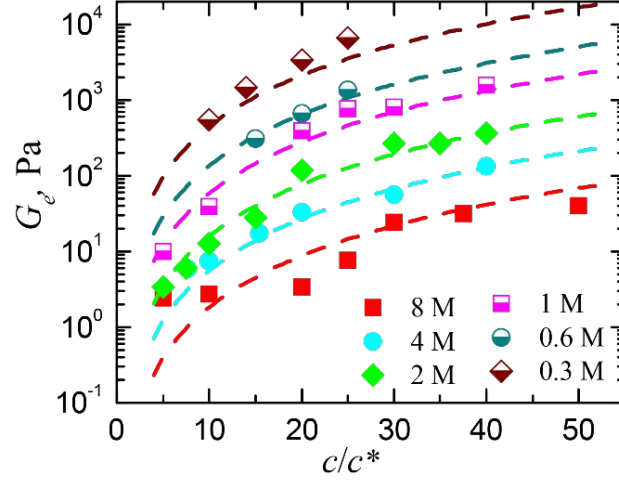
Figure S5. The experimentally obtained plateau moduli G_e as a function of normalized concentrations for 8 M, 4 M, 2 M, 1 M, 0.6 M and 0.3 M PEO, respectively. The dashed curves are the theoretical predictions based on $G_e = k_B T/L^3$ for each Mw.

S3 Calculation of the hopping time τ_{hop}

Two counterintuitive experimental findings mentioned above should be emphasized here: 1) an earlier transition from sub-diffusive regime to long-time linear regime, and 2) an enhanced diffusivity in entangled solutions with higher Mw. These are attributed to the existence of an activated hopping of "large" NP subjected to the constraint of crowded polymer networks. Figure 3c illustrates these effects. Based on these facts, we propose our approach to calculate the typical hopping timescale τ_{hop}.

The measured MSD $\langle r^2(t)\rangle_{exp}$ manifests an earlier transition (τ_c) and deviates from the prediction based on long-time reptation due to hopping. According to the fits based on Maxwell model (which is valid for Maxwell fluids such as PEO solutions and is consistent with the generalized Stokes-Einstein relation) as shown in Figure 2b in the main text, the long-time linear part of the measured MSD can be expressed as:

$$\langle r^2(t)\rangle_{exp} \approx \frac{k_B T}{\pi d G_e} t \Big/ \tau_c \tag{S1}$$

In addition, the presence of hopping introduces an additional contribution on the MSD. The linear part of the measured MSD is then actually a sum of two parts:[10]

$$\langle r^2(t)\rangle_{exp} = \langle r^2(t)\rangle_{rep} + \langle r^2(t)\rangle_{hop} \tag{S2}$$

The Maxwell model also assumes a linear MSD scaling at long-time stage since $t > \tau_{rep}$:

$$\langle r^2(t)\rangle_{rep} \approx \frac{k_B T}{\pi d G_e} \left. t \middle/ \tau_{rep} \right. \tag{S3}$$

Using τ_{hop} as the typical timescale of hopping, the MSD resulted from hopping dynamics can be similarly written as:

$$\langle r^2(t)\rangle_{hop} \approx \frac{k_B T}{\pi d G_e} \left. t \middle/ \tau_{hop} \right. \tag{S4}$$

Thus, one obtains the equation of τ_{hop}:

$$\frac{1}{\tau_{hop}} = \frac{1}{\tau_c} - \frac{1}{\tau_{rep}} \tag{S5}$$

Based on Equation S5, all the measured values of τ_{hop} can be calculated, as listed in Table S3.

Table S3. The calculated values of τ_{hop} of 200 nm NP for various PEO Mw and c

Mw [g/mol]	c^* [wt.%]	τ_{hop} [s]			
		$10c^*$	$20c^*$	$30c^*$	$40c^*$
8 M	0.040	0.035	0.17	0.23	0.34
4 M	0.065	0.0051	0.015	0.041	0.099
2 M	0.10	0.0059	0.0068	0.030	0.075
1 M	0.18	0.0058	0.0062	0.061	0.073

Also, as mentioned in Figure 1b, we measured the mean time interval between successive hops. For each cases, we used data containing hundreds of NPs to get the statistical mean value of Δt_{hop}. Table S4 displays the measured values of Δt_{hop}, which shows the good agreement with the values of τ_{hop} obtained by our approach. The measured value of the hopping interval is significantly dependent on the observation time resolution and requires a large number of data to

achieve a reliable statistical result. As a result, we can only measure Δt_{hop} for the case of large MW and c.

Table S4. Several measured values of Δt_{hop} for 200 nm NP.

Mw [g/mol]	c^* [wt.%]	Δt_{hop}		
		$20c^*$	$30c^*$	$40c^*$
8 M	0.040	0.11	0.25	0.45
4 M	0.065	0.03	0.05	0.11

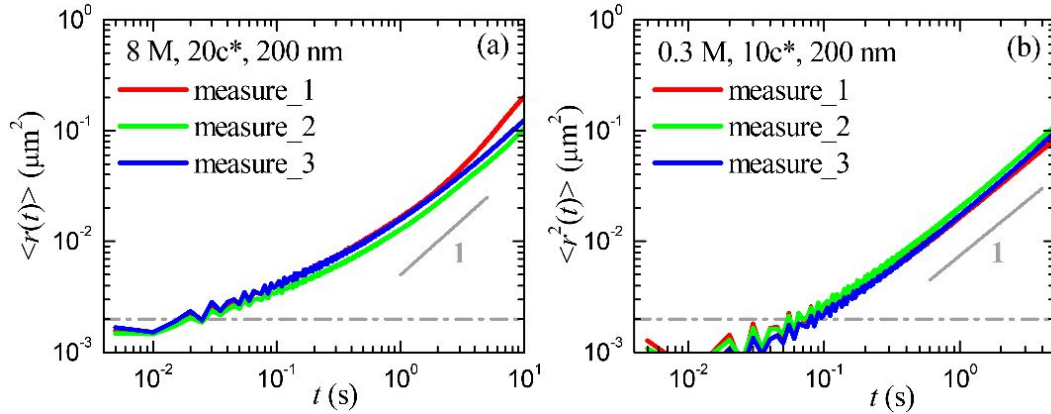## S4 Estimation of the measurement uncertainty

Figure S6. The three independent measurements of MSD for 200 nm NP in (a) 8 M ($c = 20c^*$), and (b) 0.3 M ($c = 10c^*$) PEO, respectively. Grey dash-dot lines represent the cutoff value of 0.002 μm².

In current particle tracking measurement, the centroid resolution is about $\theta \approx 0.2$ pixel by refining the locations of the local maxima of intensity (Figure S2), thus the uncertainty of the measured MSD is principally $2\theta^2 \approx 0.002$ μm². In Figure 2A, the measured MSD of 20c* - 8 M below this cutoff value shows some fluctuation at short times $t \leq 0.1$ s. However, this fluctuation will not introduce large uncertainty into determining τ_c by fitting the Maxwell model with data

from short times to long times. All the results of other *Mws* also satisfy this argument. For most situations, we performed three independent experiments. As shown in Figure S6, the divergences among the three measurements are small. To cover the uncertainty at the largest degree, we estimate that the measurement uncertainty of MSD is within 30% of its average value in the short-time region. The overall estimation of the uncertainty of MSD and τ_c are estimated to be about 15%.

In the bulk rheological measurement, the cross points of G' and G'' (coordinate value corresponding to $1/\tau_{rep}$) in different measurements vary slightly. Taking 8M, 20c* PEO as example, in three different measurements, we obtain $\tau_{rep} \approx 1.67$, 3.03 and 4.09, respectively. Accordingly, we estimate that the uncertainty of τ_{rep} is about 40% of its average value based on the standard deviation of the data.
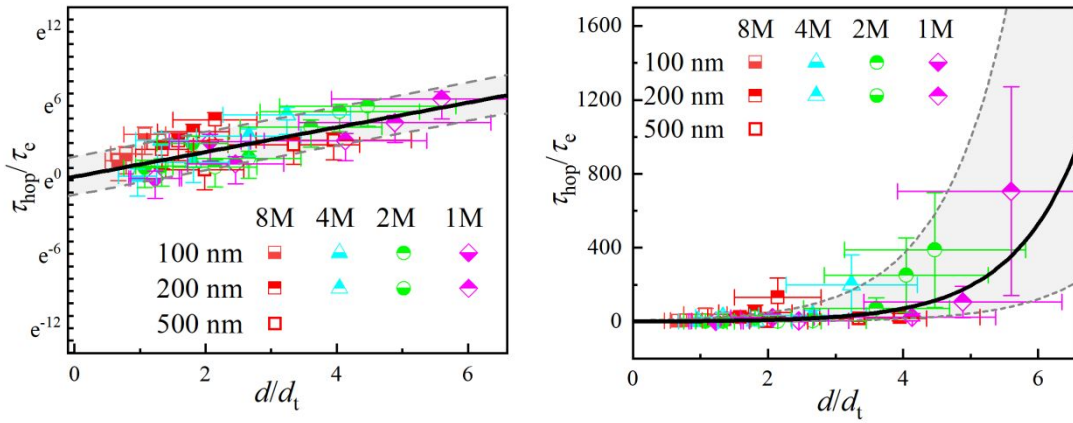

Figure S7 A plot of Figure 5 with error bars and the marked upper and lower bounds to show the tendency (left), and a linear plot of Figure 5 (right). The error bars represent the measured uncertainties.

We introduce here the uncertainty analysis of other measured data based on uncertainty propagation. For instance, based on the equation $\tau_{rep} = \tau_0(N^3/N_e(1))c^{3(1-\nu)/(3\nu-1)} \sim c^{1.5}Mw^3$, the relative uncertainty of τ_{rep}, written as $\delta\tau_{rep}/\tau_{rep}$, is estimated to be about 40% by the propagation of the uncertainties from c ($\delta c/c \sim 10\%$) and Mw ($\delta Mw/Mw \sim 10\%$). Then the uncertainty of τ_{hop} can be roughly estimated to be 60% according to $1/\tau_{hop} \sim 1/\tau_c - 1/\tau_{rep}$. By the same approach, we obtain the uncertainties of the variables τ_{hop}/τ_e and d/d_t in Fig. 5 to be up to 80% and 30%, respectively. In Table S5, we list the estimations for all the involved parameters. Then we can plot the error bars and the upper and lower bounds with the data of Fig. 5 to show the good tendency in Figure S7. A linear plot with the data from Fig. 5 and the error bars estimated above is also provided to show the data are actually within an exponential tendency.

Table S5. Estimation of the relative uncertainties

variable	d	c	Mw	d_t	τ_c	τ_e
uncertainty	5-10%	5-10%	10%	20-25%	15%	20%
variable	τ_{rep}	τ_{hop}	τ_{hop}/τ_e	d/d_t		
uncertainty	40%	60%	80%	30%		

References

1.   Omari, R. A.; Aneese, A. M.; Grabowski, C. A.; Mukhopadhyay, A. Diffusion of Nanoparticles in Semidilute and Entangled Polymer Solutions. *The Journal of Physical Chemistry. B* 2009, 113, 8449-8452.

2.   de Gennes, P.-G. *Scaling Concepts in Polymer Physics*. Cornell University Press: Ithaca, 1979.

3.   Rubinstein, M.; Colby, R. H. *Polymer Physics*. Oxford University Press: New York, 2003.

4.   de Kort, D. W.; Rombouts, W. H.; Hoeben, F. J. M.; Janssen, H. M.; Van As, H.; van Duynhoven, J. P. M. Scaling Behavior of Dendritic Nanoparticle Mobility in Semidilute Polymer Solutions. *Macromolecules* 2015, 48, 7585-7591.

5.   Sprakel, J.; van der Gucht, J.; Cohen Stuart, M. A.; Besseling, N. A. Brownian Particles in Transient Polymer Networks. *Phys Rev E Stat Nonlin Soft Matter Phys* 2008, 77, 061502.

6.   Larson, R. G. *The Structure and Rheology of Complex Fluids*. Oxford University Press: New York, 1999.

7.   Guo, H.; Bourret, G.; Lennox, R. B.; Sutton, M.; Harden, J. L.; Leheny, R. L. Entanglement-controlled Subdiffusion of Nanoparticles within Concentrated Polymer Solutions. *Phys Rev Lett* 2012, 109, 055901.

8.   van Zanten, J. H.; Amin, S.; Abdala, A. A. Brownian Motion of Colloidal Spheres in Aqueous PEO Solutions. *Macromolecules* 2004, 37, 3874-3880.

9.   Doi, M.; Edwards, S. F. *The Theory of Polymer Dynamics*. Oxford University Press: New York, 1988.

10.   Cai, L. H.; Panyukov, S.; Rubinstein, M. Hopping Diffusion of Nanoparticles in Polymer Matrices. *Macromolecules* 2015, 48, 847-862.